Palaeogeography, Palaeoclimatology, Palaeoecology 659 (2025) 112626

Contents lists available at ScienceDirect

Palaeogeography, Palaeoclimatology, Palaeoecology

journal homepage: www.elsevier.com/locate/palaeo

Pyrogenic carbon records of Holocene fire dynamics in the Yellow River Basin: Climate change and human activity forcing

Chuchu Zhang [a,b,c], Yifei Qiu [a,d], Chenglong Wang [a,b,e], Qinya Fan [a], Ziyue Feng [a], Xinqing Zou [a,b,c,*]

[a] School of Geographic and Oceanographic Sciences, Nanjing University, Nanjing 210093, China
[b] Ministry of Education Key Laboratory for Coast and Island Development, Nanjing University, Nanjing 210093, China
[c] Collaborative Innovation Center of South China Sea Studies, Nanjing University, Nanjing 210093, China
[d] Key Laboratory of Coastal Zone Exploitation and Protection, Ministry of Natural Resources, Nanjing 210024, China
[e] State Key Laboratory of Marine Geology, Tongji University, Shanghai, China

ARTICLE INFO

Edtior Name: Zhengquan Yao.

Keywords:
Fire history
Yellow River Basin
BC
PAHs
Climate change
Human activities
Carbon sequestration

ABSTRACT

Fire is a crucial component of Earth's ecosystems, with important environmental and socioeconomic implications. In this paper, we analyze black carbon and polycyclic aromatic hydrocarbons in a sediment core (YS-A) from the South Yellow Sea to investigate the driving forces of fire activity in the Yellow River Basin since 7.0 ka BP, when sea level stabilized and the modern pattern of ocean circulation system established. Our results indicate that fire activity gradually increased between 7.0 and 4.0 ka BP, reaching its highest level around 4.0–3.5 ka BP, and weakened between 3.5 and 0.5 ka BP, before rapidly increasing again after 0.5 ka BP. Climate change was found to be the dominant factor influencing fire history, with drier climatic conditions promoting fire activity during 7.0–4.0 ka BP, but suppressing it after 4.0 ka BP. This varied response of fire to climatic conditions is linked to the complex interaction between rainfall, vegetation cover, and fuel availability. Human activity is also shown to exert a complex impact, with some activities, such as deforestation, reducing vegetation cover and limiting fire activity over Late Holocene timescales, while other factors, such as coal burning, increasing high-temperature combustion since 0.5 ka BP. Furthermore, our findings suggest that fire activity has significantly influenced carbon sequestration in marine sediments, leading to an increase in the burial of refractory carbon from approximately 12 % to 18 % between 7.0 and 3.5 ka BP, and a higher proportion of terrestrial organic matter.

1. Introduction

Fire has been an integral part of Earth's ecosystems since the emergence of vegetation on land in geological history (Scott, 2000). Fire emissions of carbon dioxide (CO_2) and other greenhouse gases contribute to atmospheric composition and climate warming (Hao et al., 1996). The burning of surface plant residues by fire accelerates the carbon cycle, and fire has a significant impact on the global carbon cycle (Bowman et al., 2009). There are ecosystems where fire has been a natural factor for thousands of years, such as the Mediterranean ecosystem (Keeley et al., 2011). Additionally, fire can influence the succession of natural landscapes and ecosystems (Bond-Lamberty et al., 2007). Fire can also have detrimental effects on the environment, particularly during extreme fire activity. Over the past few decades, there has been a significant increase in the incidence of large, uncontrolled fires, leading to substantial economic, social, and ecological impacts (Bowman et al., 2017). For instance, tropical forest fires in Southeast Asia resulted in economic losses of nearly $U.S. 8.8 to 9.3 billion in 1997 (Bowman et al., 2009). Wildfires account for ~25 % of the world's forest fire and ~ 8 % of premature deaths due to poor air quality (Lelieveld et al., 2015). Therefore, the study of fire activity has significant environmental and social implications.

The occurrence of fire is dependent on three key components: sufficient combustible materials, suitable climatic background, and triggering conditions (Krawchuk et al., 2009). Climate change plays a crucial role in determining vegetation productivity, burning season, and the spread and evolution of fires (Scott and Glasspool, 2006; Huang et al., 2020; Huang et al., 2023). Additionally, human activities are

* Corresponding author at: School of Geographic and Oceanographic Sciences, Nanjing University, Nanjing 210093, China.
E-mail address: zouxq@nju.edu.cn (X. Zou).

https://doi.org/10.1016/j.palaeo.2024.112626
Received 17 June 2024; Received in revised form 7 November 2024; Accepted 9 November 2024
Available online 29 November 2024

closely related to the occurrence of fire (Pei et al., 2020; Garcés-Pastor et al., 2022). The temporal and spatial distribution of fire can be influenced by both climate change and human activities, and the dynamics of fire in geological history can provide insight into the evolution of climate change and human activities. By clarifying the interrelationships among fire, climate, vegetation, and human activities in the geological record, we can enhance our understanding of the mechanisms that drive fire occurrence and improve our predictive capability regarding future fire events.

The relationship between fire, climate, vegetation, and human activities is not yet fully understood and can vary depending on different spatial and temporal scales (Whitlock et al., 2015). Some studies suggest that fire occur more frequently in dry climates due to enhanced fire-prone weather and reduced fuel moisture (Tan et al., 2015; Heymann et al., 2017), while others suggest that the increase in temperature and humidity may have strengthened regional fire activity with more biomass burning (Han et al., 2012; Daniau et al., 2013). Additionally, some records suggest that human fire use has increased the incidence of local fires (Zong et al., 2007; Marlon et al., 2008; Thevenon et al., 2010), while others show that increased human activities has led to a general decrease in forest cover, resulting in a decrease in fire activity (Pei et al., 2020; Sun et al., 2022a). Currently, the impact of human activities on fire remains controversial, primarily due to the lack of adequate regional fire reconstruction from sediment records.

Numerous environmental proxies can be utilized for reconstructing fire history, including charcoal, black carbon (BC), tree-ring fire scars, polycyclic aromatic hydrocarbons (PAHs), and levoglucosan. BC is generated by incomplete combustion of fossil fuels and biomass, and is commonly used as a proxy for fire reconstruction (Han et al., 2012; Tan et al., 2015). The concentration of BC in sediments is generally positively correlated with fire frequencies, and the stable carbon isotopic compositions of BC ($\delta^{13}C_{BC}$) has been increasingly used for paleo-vegetation reconstructions (Pang et al., 2021; Ning et al., 2022). However, smaller variations in BC content were observed depending on the techniques used or the laboratories conducting the measurements (Hammes et al., 2007). These discrepancies can arise from differences in methodology, calibration, and sample handling, underscoring the importance of standardization in BC analysis for accurate comparisons. PAHs have also been considered as a potential proxy for reconstructing fire history (Tan et al., 2020). PAHs are widely present in marine sediments and are primarily sourced from natural forest fires and volcanic eruptions, as well as emissions from anthropogenic burning of biomass (Menzie et al., 1992; Tan et al., 2020). Furthermore, BC and PAHs have the potential to provide fire record in their source region (Burns et al., 1997; Pei et al., 2020).

The Yellow River basin is widely recognized as the cradle of Chinese civilization where the Xia Culture of the early Bronze Age founded their chieftain states and walled towns in the loess region approximately 4.0 ka BP (Huang et al., 2009). Therefore, Yellow River Basin is of great importance for understanding the past socio-environmental interactions. The South Yellow Sea (SYS) is a significant river-dominated marginal sea that receives substantial sediment loads from the Yellow River. The South Yellow Sea mud deposit (SYSMD) is one of the largest mud deposits on the SYS shelf (Fig. 1). It is characterized by the successive accumulation of fine-grained sediments, considerable thickness, and a complex dynamic environment (Ai et al., 2022), making it an ideal location for tracing the climate change and evolution of the Yellow River civilization in China. There are numerous studies about the reconstructed fire or vegetation of the Yellow River Basin from loess (Huang et al., 2006; Wang et al., 2012; Wang et al., 2018), lakes (Xiao et al., 2004; Wang et al., 2013) or marginal seas (Chen et al., 2022; Sun et al., 2022a). However, most studies only used a single proxy, which may lead to uncertainty in the results. Meanwhile, numerous studies have highlighted the significance of human impact on fire dynamics (Zong et al., 2007; Marlon et al., 2008; Pei et al., 2020), but the commencement times remains controversial. In this study, we aim to reconstruct the history of fire and vegetation change in the Yellow River Basin using high-resolution BC (content and $\delta^{13}C_{BC}$) and PAHs records from YS-A cores in the SYSMD since 7.0 ka BP, when sea level reached its present level and stabilized (Liu et al., 2004) and the modern circulation

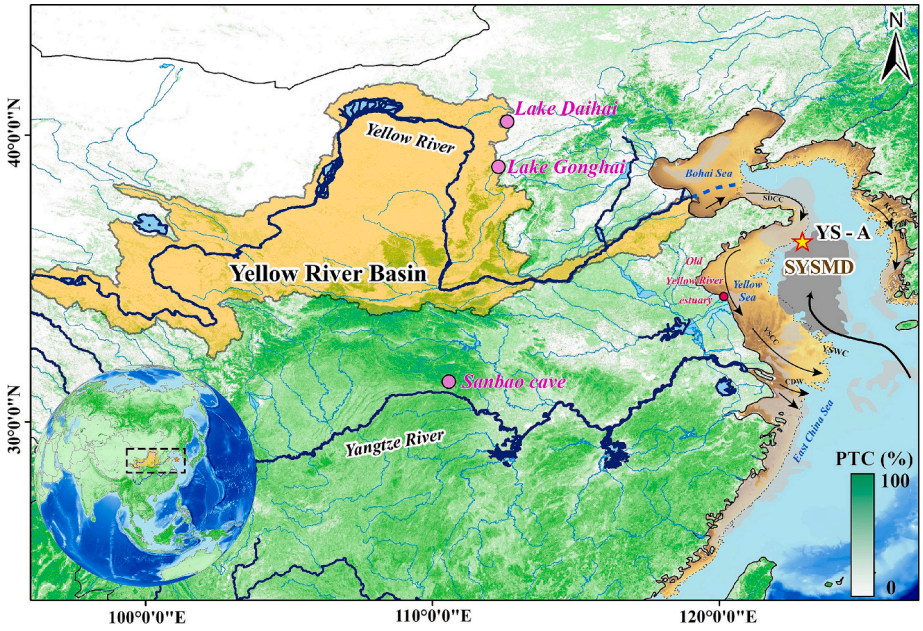

Fig. 1. Map showing the study area, location of core YS-A (yellow pentagram), surface current system (black arrows) around the area and locations of sediment core studied previously (pink circles): Sanbao Cave (Wang et al., 2008), Lake Daihai and Lake Gonghai (Sun et al., 2022b). The coastline was moved to the approximate position of present 40 m isobaths at 11.0 ka BP (Liu et al., 2004; the palo and present coastline is shown in black dotted line and black line), and proximal subaqueous delta along the northern coast of the Shandong Peninsula (orange area) developed. The blue dashed line indicates the possible location of the Paleo-Yellow River estuary. Dark gray area indicates the South Yellow Sea mud deposit (SYSMD), and light gray area indicates the mud deposit in eastern Chinese marginal seas. (For interpretation of the references to colour in this figure legend, the reader is referred to the web version of this article.)
Note: Percentage of forest coverage (PTC) data was prepared using MODIS data, covering the globe in a 500 m (15 s) interval grid (version 2).

system formed (Yang et al., 2003). We also discuss the relationship between fire, vegetation, climate change, and human activities, and evaluate the relative importance of climate change and human activities on fire in the Yellow River Basin during different periods of Holocene. Additionally, we explore the effect of fire on carbon sequestration by combining organic carbon indicators.

2. Material and methods

2.1. Study area

As the second largest river in China, the Yellow River flows through arid and semi-arid regions in the temperate zone, with an annual runoff of 890 × 10^8 m^3 and an annual sediment load of over 109 tons (Saito et al., 2001). Statistical analysis of MODIS active fire data from 2001 to 2020 reveals that an average of 223 active fires occur annually on the Chinese Loess Plateau (Zheng et al., 2024). The spatial distribution patterns of both the frequency and intensity of active fires on the Loess Plateau are similar, with a significant concentration observed in the eastern plains along the Yellow River, where agricultural land predominates and fire intensity is elevated (Zheng et al., 2024). The Yellow River Basin has garnered significant interest from the scientists for investigating Holocene climate variability and its implications for local ecosystems and human society (Huang et al., 2009). Archaeological and historical evidence indicated that the Chinese Loess Plateau, located in the upper and mid-reaches of the Yellow River Basin and currently characterized by steppe and grassland vegetation, was once covered by a forest-dominated ecosystem during the mid-Holocene (Shi, 1991).

The SYS represents typical river-dominated ocean margin, where substantial quantities of sediment are transported and deposited from the Yellow River. The sea level of the SYS at 11 ka BP was about 40 m below the present level (Liu et al., 2004). At approximately 7.0 ka BP, the sea level reached its highest level and stabilized, and the Yellow River estuary receded to its present position following transgression (Fig. 1). The modern circulation system consisting of the Yellow Sea Warm Current (YSWC), the Yellow Sea Coastal Current (YSCC), and Korean Coastal Current (KCC), the Shandong Coastal Current (SDCC), and the Changjiang Diluted Water (CDW) was formed (Fig. 1; Yuan et al., 2008). Meanwhile, the SYSMD gradually developed owing to the trapping effect of the modern circulation system (Yang et al., 2003), and undergone a two-phase process of “storage in summer and transportation in winter”.

2.2. Material

The sediment core YS-A (122.9°N, 36.3°E) was collected from SYSMD (Fig. 1) using a gravity column with an inner diameter of 110 cm in the November of 2019. The water depth of YS-A is 64.8 m and the length of core is 240 cm. The core was subsampled at 1 cm intervals to yield 240 core sediment samples and stored at −20 °C in the lab. The homogeneous olive brown clay slit of the core is indicative of a stable sedimentary environment with sufficient sediment supply.

2.3. Methods

2.3.1. Core chronology

The age model of core YS-A was established through accelerator mass spectrometry (AMS) ^{14}C dating of twelve mixed benthic foraminifera at Pilot National Laboratory for Marine Science and Technology (Qingdao). All dates were calibrated to calendar years before “present” (before 1950 CE, or BP) using the CALIB 8.20 program with an updated calibration curve Marine20, and a constant average global reservoir age of 400 years was assumed. The correction factor Delta R was −173 ± 88 yr and detailed methods were shown in Zhang et al. (2024). To optimize the available dates, age-depth modeling was carried out by Bayesian analysis using the Bacon program in R with the default settings (Blaauw and Christen, 2011).

2.3.2. Grain size

Grain size analyses were measured with a laser diffraction particle size analyzer (Mastersizer 2000, Malven Instruments Ltd., UK) from 0.02 to 2000 μm. The measuring error was within 3 %. All the samples were washed with 10 % H_2O_2 and 1 mol/L HCl for 24 h to remove the organic matter and biogenic carbonate, and immersed in sodium metaphosphate for 24 h prior to grain size analyses.

2.3.3. Black carbon

All samples were analyzed for BC and $\delta^{13}C_{BC}$, following the dichromate oxidation method (Bird and Grocke, 1997). Approximately 2 g freeze-dried samples were weighed and dissolved with a solution of 10 % HCl to remove carbonate. Then, the silicate minerals and refractory oxides were sequentially dissolved using mixture solution of HF/HCl (*v*/v, 1:1) at 85 °C. Each step reacted for 24 h. Finally, the acid-treated samples were oxidized by a mixed solution of 0.1 mol/L $K_2Cr_2O_7$ and 2 mol/L H_2SO_4 at 60 °C for 120 h to remove the kerogen fraction. Samples were washed to a neutral pH between each treatment. The final residue was washed with ultrapure carbon-free water and methanol successively, dried under room temperature, and ground into a fine powder. The process of centrifugation and rinsing was carefully repeated 3 to 6 times after each step. The remaining refractory carbon in the residue was operationally defined as BC (Pei et al., 2020). The BC concentration and $\delta^{13}C_{BC}$ value were determined using a Thermo Flash 2000 elemental analyzer interfaced with a MAT253 isotope ratio mass spectrometer. The chemical pretreatment and isotopic measurements were completed in the Third Institute of Oceanography, Ministry of Natural Resources. Replicate analysis showed that the relative error was within 5 % for BC content. Reproducibility of the standard sample was better than ±0.2 ‰ for $\delta^{13}C_{BC}$.

2.3.4. PAHs

All samples were analyzed for PAHs, following the method from Wang et al. (2015). Ultrasonication extractions were performed on 5 g of surface sediment spiked with surrogate standards (i.e., naphthalene-d_8, acenaphthene-d_{10}, phenanthrene-d_{10}, chrysene-d_{12}, and perylene-d_{12}) in 30 mL of n-hexane/dichloromethane (1:1 *v*/v) utilizing four 15 min extraction cycle, after which 2 g of activated copper was added for desulphurization. The extract was concentrated to 1 mL, purified through a chromatography column with 3 cm of neutral alumina, 3 cm of silica gel, and 1 cm of anhydrous sodium sulphate, and then eluted with 30 mL of n-hexane/dichloromethane (1:1 v/v). The eluate containing the PAHs was vacuum-evaporated and solvent-exchanged with n-hexane and finally concentrated to 500 μL under a gentle nitrogen stream.

The concentrations of 16 PAHs were analyzed by gas chromatography/triple quadrupole mass spectrometry (GC–MS/MS, Thermo Fisher Scientific, TSQ 8000 Evo, USA), fitted with a quartz capillary TG-5MS column (30 m × 0.25 mm internal diameter, 0.25 μm film thickness). The GC temperature was initially set at 80 °C and held for 2 min, then increased to 180 °C at a 20 °C/min rate for 5 min, and finally increased to 290 °C at a 10 °C/min rate for 15 min. The interface, injection and ion source temperatures were 290, 290 and 230 °C, respectively. Helium was used as the carrier gas with a flow rate of 1 mL/min. All samples were analyzed via the selected reaction monitoring (SRM) method. The chemical pretreatment and content test were completed in the Key Laboratory of Coastal and Island Development of Ministry of Education, Nanjing University.

A standard mixture solution including sixteen priority PAHs namely naphthalene (Nap), acenaphthylene (Acy), acenaphthene (Ace), fluorine (Flu), phenanthrene (Phe), anthracene (Ant), fluoranthene (Flo), pyrene (Pyr), benzo[*a*]anthracene (BaA), chrysene (Chr), benzo[*b*]fluoranthene (BbF), benzo[*k*]fluoranthene (BkF), benzo[*a*]pyrene (BaP), indeno [1,2,3-c,d]pyrene (IcdP), dibenzo[*a*,*h*]anthracene (DahA), and bnzo[*g*,

h,i]perylene (BghiP) was purchased from Supelco (USA). All the solvents used were high-performance-liquid -chromatography (HPLC) grade.

For quality control, solvent blanks, procedure blanks, and duplicate samples were processed with every twelve-sample batch. The relative standard deviation for each replicate was <10 %, and no detectable amounts of PAHs were found in procedural blanks. The linear regression coefficients for calibration curves based on eight standard concentrations (1, 10, 25, 50, 100, 250, 400, 500 ng/L) were > 0.999. The mean surrogate recoveries were 55.90 %, 75.90 %, 83.79 %, 94.43 %, and 93.27 % for naphthalene-d_8, acenaphthene-d_{10}, phenanthrene-d_{10}, chrysene-d_{12}, and perylene-d_{12}, respectively.

2.3.5. Bulk Parameters

All the sediment samples were analyzed for total organic carbon (TOC) and stable isotope ($\delta^{13}C_{TOC}$). The freeze-dried and homogenized samples were treated with 1 M HCl to remove inorganic carbon, and then rinsed several times with deionized water to neutralize them. A Thermo Flash 2000 elemental analyzer interfaced with a MAT253 isotope ratio mass spectrometer was used to determine the TOC content and $\delta^{13}C_{TOC}$.

2.3.6. Statistical analysis

Pearson correlation analysis was used to test the strength of associations between BC/PAHs contents or climate change/human activity records after normality tests, and the statistical significance was considered for $p < 0.05$ (two tailed tests). Pearson correlation analysis were performed with SPSS software (IBM SPSS Statistics 24.0).

3. Results

3.1. Chronology

The age model for core YS-A was based on accelerator mass spectrometry (AMS) ^{14}C measurements carried out on twelve mixed benthic foraminifera. The age-depth model was determined using Bayesian analysis and presented in Table 1 and Fig. 2a. An age model developed by Zhang et al. (2024) suggests that the upper 180 cm of YA-A has been deposited since ~7.0 ka BP, corresponding to the time when sea level reached its present level and stabilized and the modern circulation system formed.

Table 1
AMS^{14}C dating and calibrated ages of sediment core YS-A.

Core depth (cm)	Material	AMS^{14}C age (yr BP)	Calibrated age (cal yr BP)	Calibrated age range 2σ (cal yr BP)
0	Mixed benthic foraminifera	410 ± 30	0	–
10	Mixed benthic foraminifera	775 ± 25	395	173–596
20	Mixed benthic foraminifera	1155 ± 20	724	531–922
40	Mixed benthic foraminifera	1545 ± 20	1112	895–1317
60	Mixed benthic foraminifera	2290 ± 70	1939	1644–2274
90	Mixed benthic foraminifera	2630 ± 20	2372	2109–2667
120	Mixed benthic foraminifera	3615 ± 40	3562	3301–3849
140	Mixed benthic foraminifera	4185 ± 30	4303	3997–4587
160	Mixed benthic foraminifera	5350 ± 30	5712	5467–5939
180	Mixed benthic foraminifera	6670 ± 40	7153	6902–7397
210	Mixed benthic foraminifera	9700 ± 30	10,697	10,393–11,057
240	Mixed benthic foraminifera	9890 ± 50	10,955	10,802–11,122

3.2. Black carbon

Fig. 2b illustrates that the BC content in core YS-A ranged from 0.55 ‰ to 1.75 ‰, with an average value of 1.18 ± 0.22 ‰. The BC content exhibited a generally low value (0.99 ± 0.22 ‰) and an increasing trend between 240 cm and 128 cm (around 11.0–4.0 ka BP), with a relatively high value between 128 cm and 115 cm (around 4.0–3.5 ka BP). The BC content slightly decreased upwards between 115 cm and 15 cm (around 3.5–0.5 ka BP), and finally exhibited an increasing trend to the top 15 cm. The $\delta^{13}C_{BC}$ values for core YS-A ranged from −23.01 ‰ to −21.15 ‰, with an average value of −21.72 ± 0.32 ‰ (Fig. 2d). The $\delta^{13}C_{BC}$ values showed a more negative value (−21.81 ± 0.29 ‰) between 240 cm and 180 cm (around 11.0–7.0 ka BP), with a relatively stable value between 180 cm and 15 cm. Finally, the $\delta^{13}C_{BC}$ values exhibited the most negative value (−22.37 ± 0.41 ‰) from 15 cm to the top.

3.3. PAHs

Fig. 2c illustrates that the concentration of PAHs in core YS-A ranged from 46.35 ng/g to 139.19 ng/g, with an average value of 91.73 ± 19.21 ng/g. The PAH content exhibited an increasing trend between depths of 240 cm and 128 cm (around 11.0–4.0 ka BP), a relatively high value between 128 cm and 115 cm (around 4.0–3.5 ka BP), a slightly decreasing trend upwards between 115 cm and 15 cm (around 3.5–0.5 ka BP), and an increasing trend to the top 15 cm. The trend of medium molecular weight PAHs (MMW PAHs, PAHs with 3–4 rings) compounds was similar to that of PAHs (Fig. 2f), whereas high molecular weight PAHs (HMW PAHs, PAHs with 5–6 rings) compounds exhibited a completely different trend (Fig. 2e). HMW PAHs had a relatively low value between depths of 240 cm and 15 cm (around 11.0–0.5 ka BP), with an obvious increasing trend and the highest value from 15 cm to the top.

4. Discussion

4.1. Provenance and implication of BC and PAHs

During 11.0–7.0 ka BP, there was a notable increase in the concentrations of BC and PAHs. The negative correlation observed between BC ($r = -0.58$, $p < 0.001$), PAHs ($r = -0.76$, $p < 0.001$), and mean grain size (Fig. S1a, b) suggests that hydrodynamic sorting played an important role in the distribution of BC and PAHs during this period. At 11.0 ka BP, the sea level of SYSMD was approximately 40 m below the current level, but it rapidly rose to its present level and stabilized at around 7.0 ka BP (Fig. 1; Liu et al., 2004). Therefore, it is likely that sea level changes influenced the distribution of BC and PAHs during 11.0–7.0 ka BP. In addition, SYSMD gradually developed owing to the trapping effect of the modern circulation system since around 7.0 ka BP (Yang et al., 2003). After 7.0 ka BP, there was no significant correlation observed between BC ($r = -0.13$, $p > 0.05$), PAHs ($r = -0.11$, $p > 0.05$), and mean grain size (Fig. S1c, d), indicating that hydrodynamic sorting was unlikely to influence the distribution of BC and PAHs during this period. In addition, the absence of correlation between BC, PAHs content and the clay, silt, sand contents suggested that BC and PAHs content was usually not influenced by sediment fractions (Table S1). Meanwhile, there has been a significant correlation between BC and PAHs content ($r = 0.65$, $p < 0.001$), which suggested that changes in BC and PAHs were homogeneous since 7.0 ka BP. Therefore, BC and PAHs content in core YS-A can closely reflect the emissions of BC and PAHs due to the fires since 7.0 ka BP.

In this study, we utilized $\delta^{13}C_{BC}$ to limit the origins of core YS-A sediments from 7.0 ka BP. The $\delta^{13}C_{BC}$ variation in core YS-A ranged from −23.01 ‰ to −21.15 ‰ (average = −21.70 ‰) since 7.0 ka BP, which was generally consistent with the range of Yellow River surface

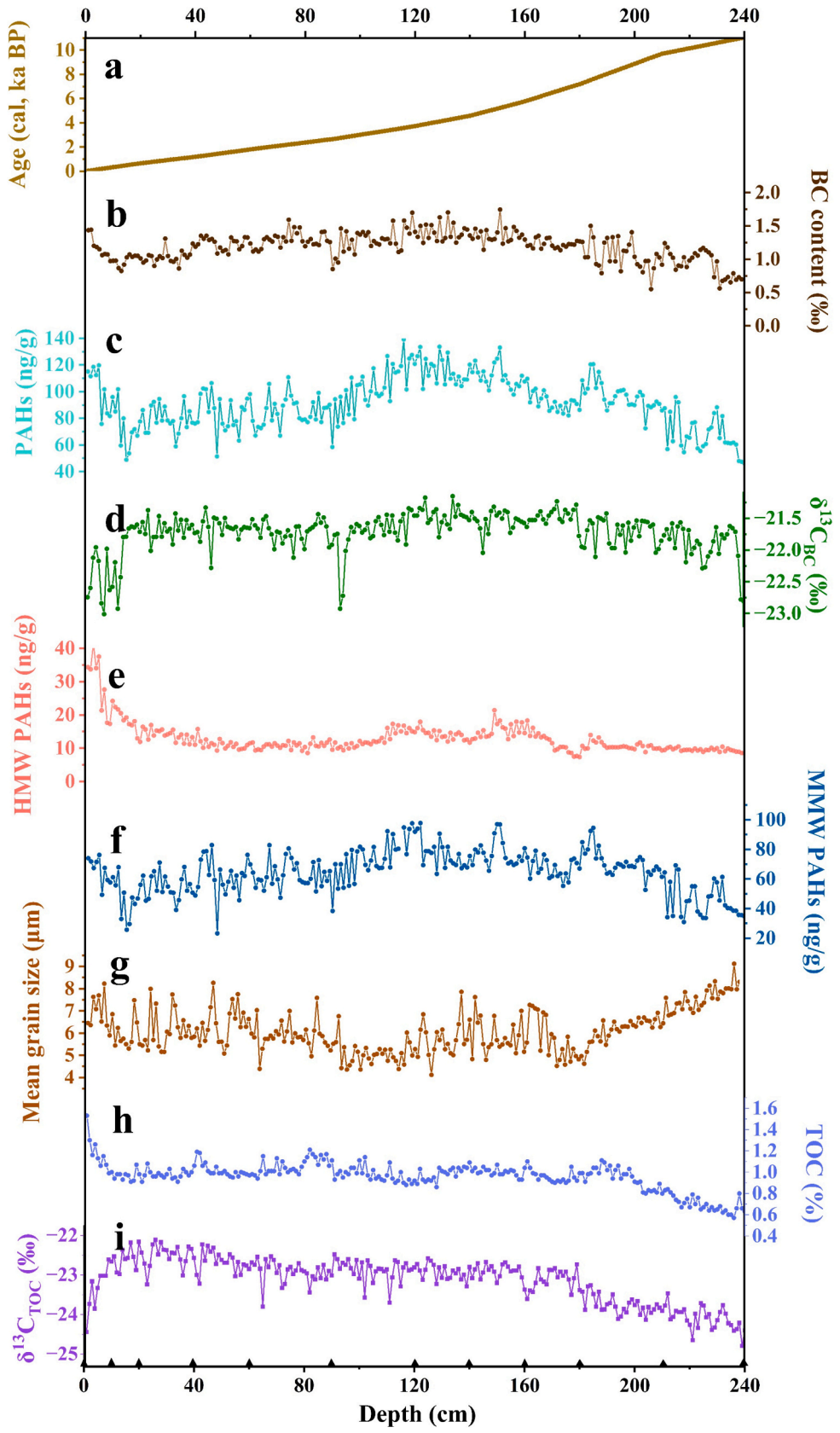

Fig. 2. Results of (a) age model; (b) BC (‰); (c) PAHs (ng/g); (d) $\delta^{13}C_{BC}$ (‰); (e) HMW PAHs (ng/g); (f) MMW PAHs (ng/g); (g) mean grain size (μm); (h) TOC (%); (i) $\delta^{13}C_{TOC}$ (‰).

sediments (from −22.6 ‰ to −20.6 ‰) (Chen et al., 2021). Furthermore, the average $\delta^{13}C_{BC}$ from the surface sediment of the Yangtze River was more positive (~ − 20.2 ‰) (Chen et al., 2021). Previous studies of clay minerals, heavy minerals and elemental geochemistry in the surface sediments also indicated that the sediments in the SYSMD were mainly transported from the Yellow River by the YSWC and YSCC, with minor delivery from the Yangtze River (Alexander et al., 1991; Yang et al., 2003; Yang and Liu, 2007). Moreover, the clay mineral composition and heavy mineralogy of sediment cores in the SYS showed that Yellow River was the major provenance of the study area, at least since MIS 3 (Liu et al., 2010; Zhang et al., 2013). Other potential sources, such as small localized rivers with a relatively low flux of suspended sediment, make a limited contribution to the study region (Milliman and Farnsworth, 2011). Therefore, we conclude that the sediments from core YS-A primarily originated from the Yellow River Basin since 7.0 ka BP. By combining the aforementioned provenance constraints, we emphasize that the content of BC and PAHs in core YS-A sediment could reflect the regional fire activity throughout the Yellow River Basin since 7.0 ka BP, rather than individual fire activity in any particular local area (Pei et al., 2020).

4.2. Fire history and sources of the Yellow River Basin since 7.0 ka BP

The concentration of BC and PAHs is positively correlated with the extent and frequency of fire (Zhou et al., 2007; Tan et al., 2020), with increases in BC and PAHs in sediments indicating more intensive fires. Our results of BC and PAHs indicate that fire activity increased gradually during 7.0–4.0 ka BP, reaching to the highest level around 4.0–3.5 ka BP, and became relatively weak until 0.5 ka BP (Fig. 3a, b). Notably, fire activity showed a rapidly rising trend since 0.5 ka BP (Fig. 3a, b). Generally, the gradual decline of fire activity since the mid-Holocene depicted by the BC and PAHs content in core YS-A (Fig. 3a, b) is consistent with records of sediment cores from the South Yellow Sea (Sun et al., 2022a), the East China Sea (Pei et al., 2020), Lake Daihai in north-central China (Wang et al., 2013) and Lake Lia in the Southern Carpathians, Romania (Finsinger et al., 2016). Meanwhile, a significant increase in fire activity from last few hundred years appears to occur in the cores from southeastern part of the Loess Plateau (Tan et al., 2015), Tianchi Crater Lake (Pang et al., 2021) and Laizhou Bay (Tan et al., 2022).

The similar production processes by BC and PAHs provide a possibility to infer the fire sources. The component of PAHs is typically used as a qualitative source identification method to explore the fate and transport of PAHs in the environment (Yunker et al., 2002) and further identify the sources of fire (Argiriadis et al., 2018; Tan et al., 2020). The components of PAHs in YS-A were primarily composed of 3–4 ring compounds, especially Phe, which were used as indicators from biomass combustion (Tan et al., 2020). Meanwhile, isomer pair ratios, including ratios of Ant/(Ant+Phe), Flo/(Flo+Pyr), IcdP/(IcdP+BghiP), and BaA/(BaA+Chr), are often used to differentiate between combustion and petroleum sources. As shown in Fig. 4, the ratios of Ant/(Ant+Phe) and Flo/(Flo+Pyr) were greater than 0.1 and 0.5 for most samples, respectively. The ratios of BaA/(BaA+Chr) and IcdP/(IcdP+BghiP) were greater than 0.3 and 0.5 for most samples, respectively. In summary, the ratios of Ant/(Ant+Phe), Flo/(Flo+Pyr), IcdP/(IcdP+BghiP), and BaA/(BaA+Chr) in core YS-A suggest that the majority of PAH components in most samples may have originated from pyrogenic sources and biomass burning (Yunker et al., 2002), which is consistent with a previous study in the middle reaches of the Yellow River drainage basin (Tan et al., 2020). Additionally, $\delta^{13}C_{BC}$ values can provide information on the type of vegetation consumed (Bird and Grocke, 1997). Liu et al. (2013) reported that C4% values less than 32.1 % based on measured $\delta^{13}C_{SOC}$ values for surface soil samples in the Chinese Loess Plateau. Additionally, Wang et al. (2013) used $\delta^{13}C_{BC}$ values of −26.3 ‰ and − 13.0 ‰ as end-member values for BC produced from C3 and C4 plants during the Holocene in the Chinese Loess Plateau. Consequently, the average $\delta^{13}C_{BC}$ value of −21.69 ‰ throughout the YS-A record suggests that the vegetation in the Yellow River Basin has been primarily composed of C3 plants since 7.0 ka BP, aligning with previous studies (Liu et al., 2011; Wang et al., 2013).

4.3. Influence of climate change on fire dynamics since 7.0 ka BP

The occurrence of fire can be directly and indirectly influenced by climate change, specifically changes in precipitation and temperature. Directly, climate change can affect fire through its impact on ignition, fuel moisture, and fire temperature; indirectly, it influences fire dynamics through alterations in vegetation composition and productivity (Daniau et al., 2010). We found a decreasing trend of precipitation inferred from Sanbao Cave speleothem isotopic records (Wang et al., 2008) (Fig. 3g), pollen-based moisture index in the Yangtze River Basin (Zhao et al., 2009) (Fig. 3i) and annual precipitation in northern China (Chen et al., 2015) (Fig. 3i) but an increasing trend of fire activity between 7.0 and 4.0 ka BP. Interestingly, after 3.5 ka BP, fire activity showed a significant trend of weakening until 0.5 ka BP. Meanwhile, there was a negative correlation between BC (Fig. 5a; $r = -0.52$, $p < 0.01$), PAHs (Fig. 5c; $r = -0.60$, $p < 0.01$) and moisture index during 7.0–4.0 ka BP, but a positive correlation between BC (Fig. 5a; $r = 0.58$, $p < 0.001$), PAHs (Fig. 5c; $r = 0.79$, $p < 0.001$) and moisture index during 4.0–0 ka BP. Besides, there was a positive correlation between BC (Fig. 5b; $r = 0.58$, $p < 0.01$), PAHs (Fig. 5d; $r = 0.66$, $p < 0.001$) and $\delta^{18}O$ (VPDB, ‰) from Sanbao cave (Wang et al., 2008) during 7.0–4.0 ka BP, but a negative correlation between BC (Fig. 5b; $r = -0.68$, $p < 0.001$), PAHs (Fig. 5d; $r = -0.82$, $p < 0.001$) and $\delta^{18}O$ (VPDB, ‰) from Sanbao cave during 4.0–0 ka BP. It may suggest that drier climatic conditions have promoted fire activity during 7.0–4.0 ka BP and suppressed the fire activity since 4.0 ka BP instead. Furthermore, we also observed the response of fire activity to global changes. By comparing the relationship between fire activity and Bond events (Bond et al., 2001), we found that the content of both BC and PAHs increased at ~4.2, ~4.6, ~5.2, and ~ 5.8 ka BP, while in the phases of ~0.4, ~1.4, and ~ 2.8 ka BP, the content of both BC and PAHs decreased (Fig. 3a, b), suggesting that the cold events before ~4.0 ka BP enhanced fire activity, whereas subsequent cold events suppressed it.

We hypothesize that the shift in the correlation of fire activity and precipitation around 4.0 ka BP in the Yellow River Basin may be primarily due to changes in vegetation cover. During 7.0–4.0 ka BP, the climate was persistently warm and humid (Wang et al., 2012) and vegetation cover was high (Fig. 3h; Sun et al., 2022b), providing sufficient fuel for fire occurrence. During this time, decreased moisture were more likely to cause fires by reducing the moisture content of fuel and increasing fuel flammability. In drier environment, the frequency of fire ignition increases (Zhang et al., 2015). Additionally, drier climate conditions are believed to have influenced cloud microphysics by increasing suspended aerosols and cloud condensation nuclei (Williams et al., 2002), leading to increased lightning activity (Price, 2009). Therefore, we speculated that fuel availability was the primary driver of fire occurrence during 7.0–4.0 ka BP. In contrast, after 4.0 ka BP, the moisture index in northern China declined (Fig. 3i; Zhao et al., 2009; Chen et al., 2015), the climate changed from wet to semi-arid (Wang et al., 2012), and the vegetation cover in Lake Daihai and Lake Gonghai was relatively low and gradually decreased (Fig. 3h; Xiao et al., 2004; Sun et al., 2022b). Consequently, productivity and fuel abundance inhibited the occurrence and spread of fire since 4.0 ka BP. Drier climate conditions limited the growth of vegetation and thus could not provide abundant fuel for the occurrence of fires. We speculated that the response of fire to climatic conditions may depended heavily on whether vegetation cover limits fire occurrence at this time, suggesting that the threshold effect of climate change on fire activity could explain the shift in fire activity in the Yellow River Basin. Our result is similar to a previous study (Sun et al., 2022a) and strongly suggest that both climate and vegetation have been the main drivers of fire activity, although the

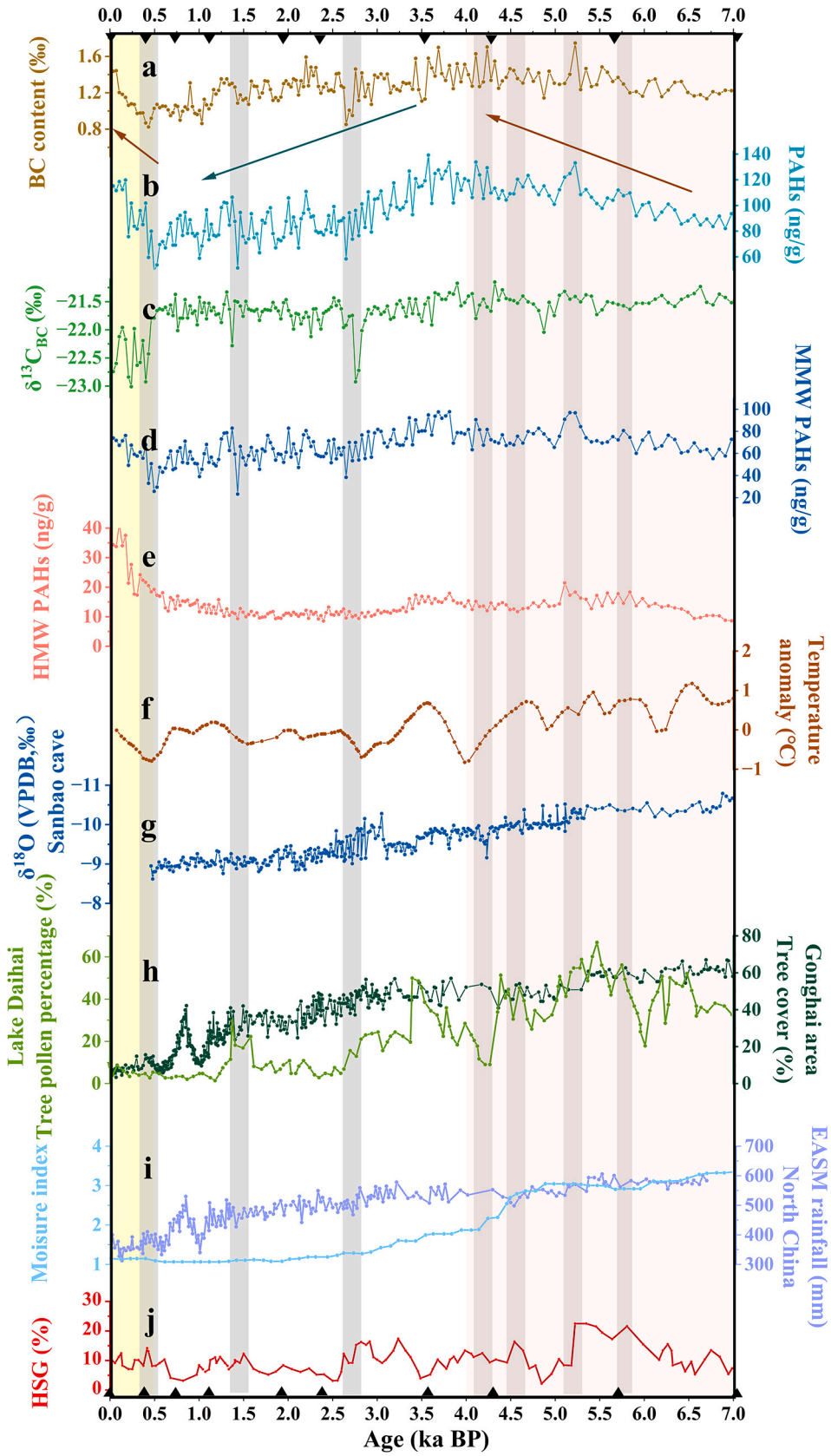

(caption on next page)

Fig. 3. Comparison of the records of fire activity with other records since 7.0 ka BP. (a) BC content (‰) of core YS-A; (b) PAHs content (ng/g) of core YS-A; (c) $\delta^{13}C_{BC}$ (‰) of core YS-A; (d) MMW PAHs content (ng/g) of core YS-A; (e) HMW PAHs content (ng/g) of core YS-A; (f) temperature anomaly record derived from China (Hou and Fang, 2012); (g) The $\delta^{18}O$ profile from Sanbao Cave in Hubei province, central China, near the southern edge of the Chinese loess plateau (Wang et al., 2008); (h) percentage of tree pollen recorded from the sediment core in Lake Daihai (Xiao et al., 2004) and Holocene record of tree cover from the Gonghai Basin in the Loess Plateau (Sun et al., 2022b); (i) moisture index-based pollen in northern China (Zhao et al., 2009) and annual precipitation in northern China (PNAA) (Chen et al., 2015); (j) Bond events as revealed by ice rafted debris (IRD) identified in the North Atlantic (Bond et al., 2001). The red and yellow rectangles show the different change trends of fire activity during 7.0–4.0 and 0.5–0 ka BP. The gray areas refer to changes of fire activity related to Bond events. The black triangles are age control points. (For interpretation of the references to colour in this figure legend, the reader is referred to the web version of this article.)

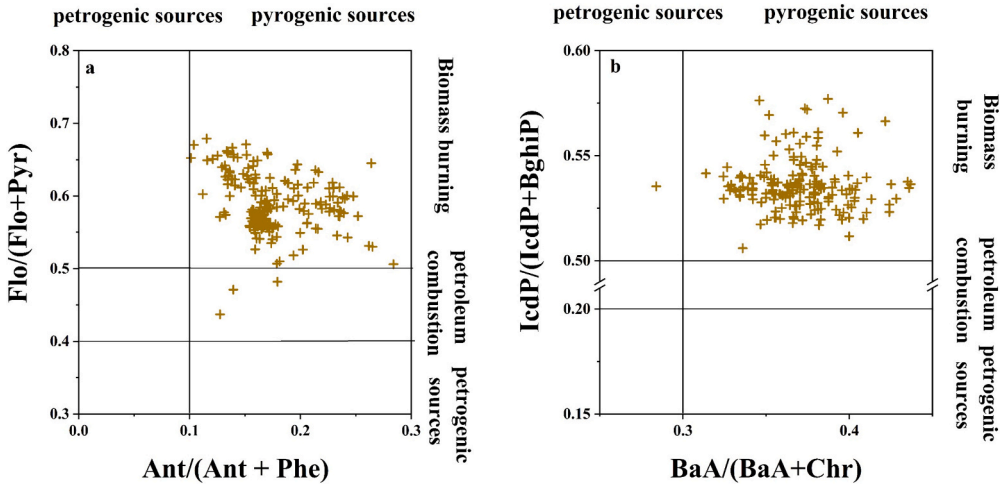

Fig. 4. The source analysis of the ratio of PAH isomers from the YS-A; (a) isomeric ratios of Ant/(Ant+Phe) and Flo/(Flo+Pyr), (b) isomeric ratios of IcdP/(IcdP+BghiP) and BaA/(BaA+Chr).

linkages are complex (Mu et al., 2017).

4.4. Fire activity in response to human activities

As mentioned above, the relationship between fire activity and climate shifted as vegetation cover decreased. In addition to the drier climate (Fig. 3g, i), human activities may also be an important cause of the decline in vegetation cover. The Xia Dynasty was founded about 4.0 ka BP, when China entered the Bronze Age. Humans used fire to attract prey, accelerate the establishment of agricultural areas, and facilitate settlement (Zong et al., 2007). Slash-and-burn techniques have been widely used to convert forests into crop fields and pastures (Mu et al., 2017). Since 4.0 ka BP, cereal-based agriculture has been widespread on the Yellow River Basin (Wang et al., 2012). In addition, previous studies suggest that anthropogenic deforestation is the main reason for the decrease in vegetation coverage to the lowest level since the Late Holocene (Fig. 3h; Sun et al., 2022b; Garcés-Pastor et al., 2022). These findings indicate that human activities may have influenced fire activity in the Yellow River Basin since the Late Holocene. Human activities, such as deforestation, cultivation, and mining, have led to a reduction in vegetation cover, which in turn has decreased the availability of combustible materials and ultimately suppressed fire activity over millennial timescales since the Late Holocene. In other words, human activities have superimposed on vegetation cover at the millennial scale to influence fire activity. In the future, the primary impact of human activities on fire activity is likely to be through anthropogenic climate change (Scholze et al., 2006; Zheng et al., 2023).

Furthermore, human activities have been observed to cause fluctuations in fire activity on a centennial scale. Specifically, during 1.9–1.8 ka BP (late Han Dynasty), 1.6–1.4 ka BP (Wei-Jin Southern & Northern Dynasties), 1.1–0.9 ka BP (Tang-Song Dynasty), the decreased BC and PAHs concentration in YS-A (Fig. 6a, b) coincided with large-scale population migrations from Northern China (the Yellow River Basin) to Southern China (the Yangtze River Basin). This finding is consistent with the trend of increasing BC content during these periods in the East China Sea (Pei et al., 2020). Meanwhile, we found that 1.4 ka BP was a cold event, and previous study also suggest that prolonged periods of cold and dry climate would result in resource depletion, warfare, dynastic succession, and population migration (Zhang et al., 2008), which is more common in Northern China with relative high latitudes (Pei et al., 2016). The large-scale population migrations from the Yellow River Basin to the Yangtze River Basin during these periods reduced the demand for land and resources, resulting in a decrease in the need for fire to clear forests for farmland and domestic uses such as cooking. Therefore, a sudden decrease in population would lead to a reduction in fire activity in the Yellow River Basin on a short-term (centennial scale).

Intuitively, $\delta^{13}C_{BC}$ became more negative, suggesting that fire may have generated more BC from C3 biomass such as wheat since 0.5 ka BP (Fig. 6c). Additionally, there was a clear trend of increasing HMW PAHs content (Fig. 6e) since 0.5 ka BP, which is not present in other time periods. We speculate that the negative $\delta^{13}C_{BC}$ is due to the rapid growth of population (Fig. 6f), which led to a significant increase in wheat cultivation. With the rapid population growth during the Ming and Qing Dynasties (since around 0.5 ka BP; Wang et al., 2006), wheat was widely cultivated in the Yellow River Basin, where cultivation techniques, processing and utilization techniques matured and wheat accounted for half of the major part of northern China (Tian, 2018). Especially, the population growth during the Qianlong era of the Qing Dynasty (around 0.2 ka BP) led to the reclamation of almost all arable land and an unprecedented increase in biomass burning on arable land, eventually forming the agricultural landscape (Cheng, 2010). In addition, historical records indicate that coal was first developed and utilized in the pre-Qin period (around 2.0 ka BP), gradually developed, and finally reached its peak in the Ming and Qing dynasties (Wu, 2010). Traditional coal mining technology was at the forefront of the world during the Ming and Qing dynasties, which also promoted the transformation of the energy structure. Hence, it is plausible that the combustion of coal has also contributed to the negative $\delta^{13}C_{BC}$ values since 0.5 ka BP. Consequently, the burning of wheat straw and coal might be responsible for the obvious negative trend of $\delta^{13}C_{BC}$ since 0.5 ka BP. Moreover, in the process of

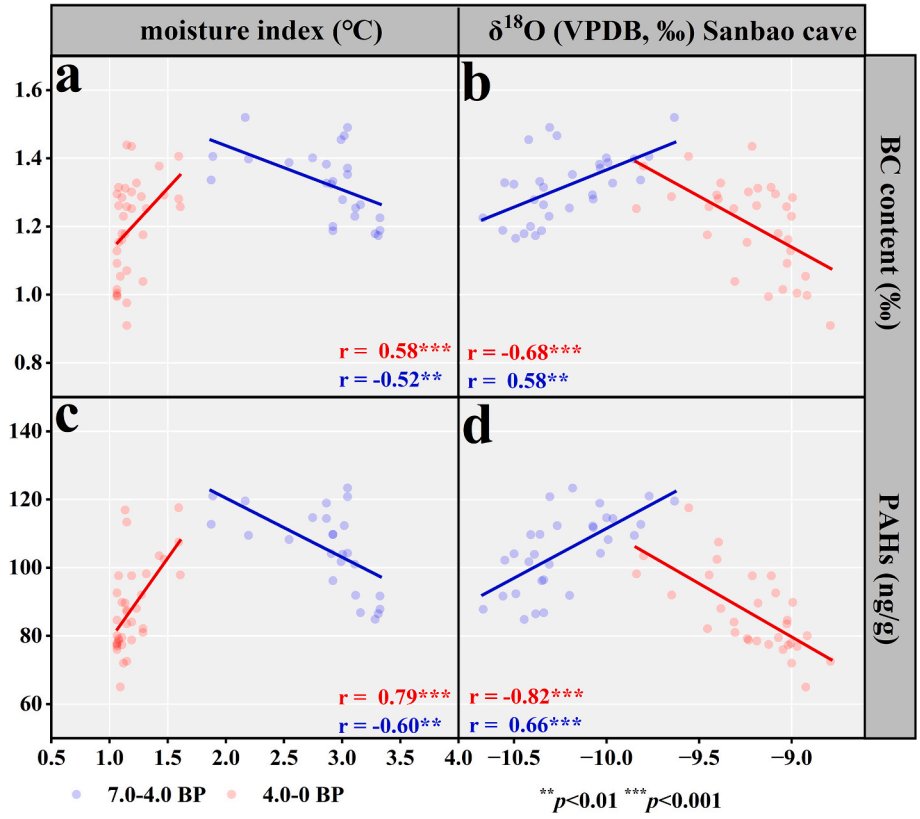

Fig. 5. Correlation analysis between climate and fire shows an abrupt change in their relationship before and after 4.0 ka BP in YS-A core. Correlations between (a) moisture index (Zhao et al., 2009) and BC content between 7.0 and 4.0 ka BP (blue line) and 4.0–0 ka BP (red line); (b) $\delta^{18}O$ (VPDB, ‰) from Sanbao Cave in Hubei province, central China, near the southern edge of the Chinese loess plateau (Wang et al., 2008) and BC content between 7.0 and 4.0 ka BP (blue line) and 4.0–0 ka BP (red line); (c) moisture index (Zhao et al., 2009) and PAHs content between 7.0 and 4.0 ka BP (blue line) and 4.0–0 ka BP (red line); (d) $\delta^{18}O$ (VPDB, ‰) from Sanbao Cave in Hubei province, central China, near the southern edge of the Chinese loess plateau (Wang et al., 2008) and PAHs content between 7.0 and 4.0 ka BP (blue line) and 4.0–0 ka BP (red line). In the figures, "**" indicates $p < 0.01$, and "***" indicates $p < 0.001$. (For interpretation of the references to colour in this figure legend, the reader is referred to the web version of this article.)

vegetation combustion, the compounds generated by different combustion temperatures are also different. The higher the combustion temperature, the more likely to produce HMW PAHs (Argiriadis et al., 2018). The apparent increase in high temperature combustion during this period is also likely due to coal burning. These findings suggest that a significant increase in human activity could promote more fire activity during specific periods in the short term.

4.5. *Effects of fire on carbon sequestration*

BC is a highly condensed, refractory and polymerized residue of combustion (Hammes et al., 2007), with a slow microbial oxidation rate (Hamer et al., 2004). Therefore, BC can be preserved in soils and sediments for thousands to millions of years (Mitra et al., 2009). The BC/total organic carbon (TOC) ratio can be used to determine the proportion of refractory components in organic carbon (Wang and Li, 2007; Ren et al., 2019), which can help us understand the burial efficiency of organic carbon. Our analysis revealed an increasing trend in the BC/TOC ratio between 7.0 and 3.5 ka BP, from approximately 12 % to 18 %, followed by a decreasing trend since 3.5 ka BP, which is similar to the trend of fire activity (Fig. 7d). We also found a positive correlation between PAHs (Fig. S2a; $r = 0.61$, $p < 0.001$) and BC/TOC ratio. These findings suggest that increased fire activity can enhance the sequestration of refractory carbon in marine sediments. Although the increased incidence of fire activity may release additional CO_2 into the atmosphere, this effect could be offset over the long term by the increased sequestration of BC in soil or sediment (Mitra et al., 2009).

Previous studies have demonstrated that nutrient addition by fire can enhance phytoplankton production (Tang et al., 2021; Liu et al., 2022), but our results seem to be different. The stable isotopic signature of organic carbon ($\delta^{13}C_{TOC}$) signature provides information on the source of organic carbon deposited at this site (Fig. 7e), as the terrestrial organic matter has a more negative $\delta^{13}C_{TOC}$ value. In the SYS, $\delta^{13}C_{TOC}$ value was approximately −20.5 ‰ and − 26.5 ‰ for marine and terrestrial organic matter (Liu et al., 2020). We observed a negative correlation between BC (Fig. S2b; $r = -0.30$, $p < 0.001$), PAHs (Fig. S2c; $r = -0.30$, $p < 0.001$) and $\delta^{13}C_{TOC}$. Our results revealed that enhanced fire activity may promote the proportion of terrestrial organic matter. We suspect that fire may promote the facilitation of soil erosion by wind or water (Sankey et al., 2009), resulting in a large number of terrestrial organic matter from rivers to the sea. SYS is an offshore sea influenced by large rivers, not an open ocean, or an offshore sea without river influence, so the impact of substantial river input may surpass the impact of phytoplankton growth stimulated by fire. In other words, the occurrence of fire may increase both terrestrial and marine organic matter, but may have a greater impact on terrestrial organic matter in the SYS, resulting in an increased proportion of terrestrial organic matter. Currently, our understanding of the effects of fire on the ocean is limited compared to our knowledge of their role in terrestrial ecosystems. Therefore, further research is necessary to analyze the relationship between fires and carbon sequestration in marine sediment.

5. Conclusions

This study aims to reconstruct a high-resolution regional fire history in the Yellow River Basin since 7.0 ka BP. Our analysis of BC and PAHs

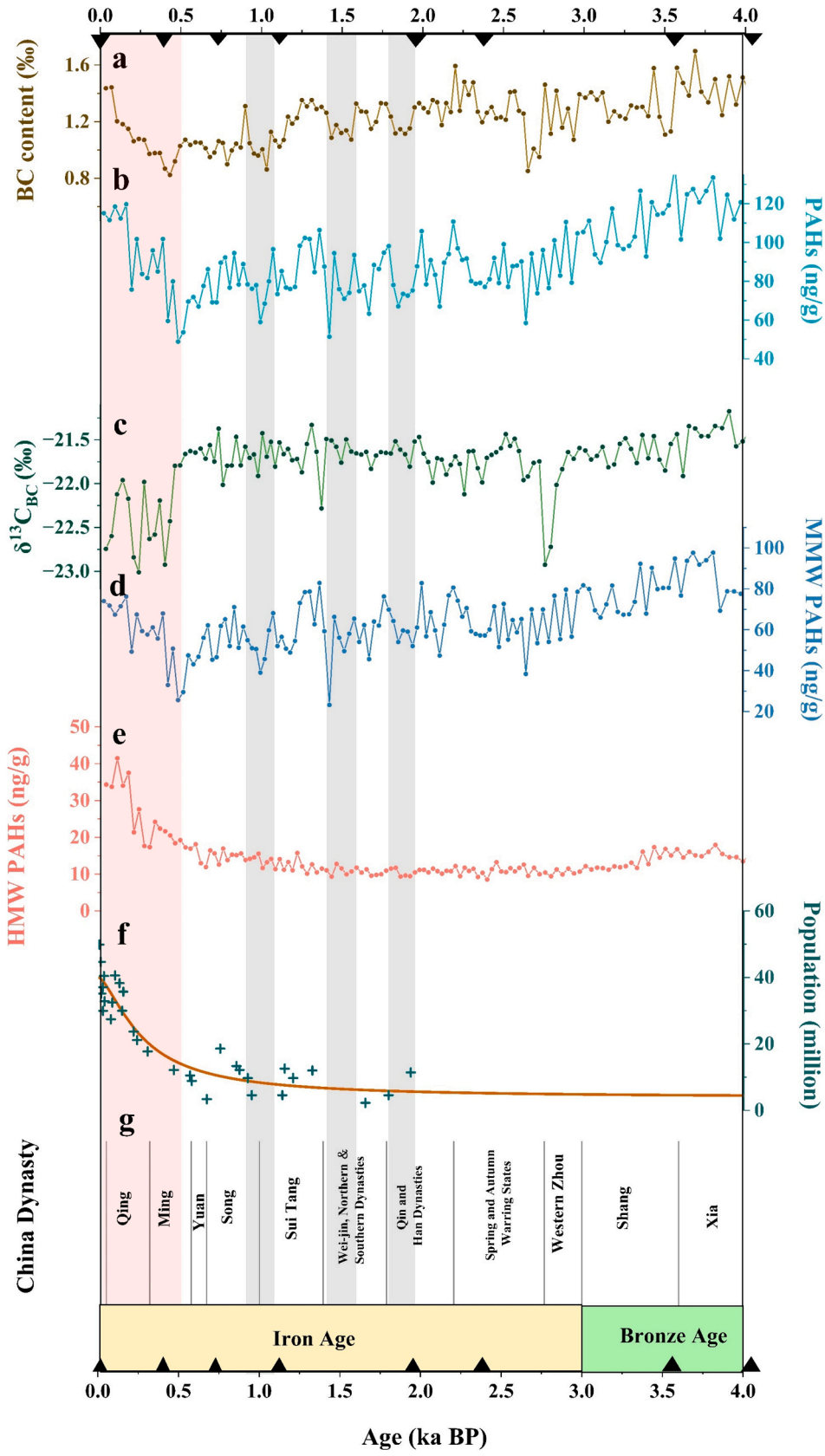

(caption on next page)

Fig. 6. Comparison of the records of fire activity with human activities since 4.0 ka BP. (a) BC content (‰) of core YS-A; (b) PAHs content (ng/g) of core YS-A; (c) $\delta^{13}C_{BC}$ (‰) of core YS-A; (d) MMW PAHs content (ng/g) of core YS-A; (e) HMW PAHs content (ng/g) of core YS-A; (f) changes of population in the Loess Plateau (Zhao et al., 2013); (g) Chinese dynasties. The gray areas refer to changes of fire activity related to large-scale population migrations from Northern China (the Yellow River Basin) to Southern China (the Yangtze River Basin). The red areas refer to changes of fire activity since 0.5 ka BP, when cultivation techniques, processing and utilization techniques matured and coal mining technology was at the forefront of the world. The black triangles are age control points. (For interpretation of the references to colour in this figure legend, the reader is referred to the web version of this article.)

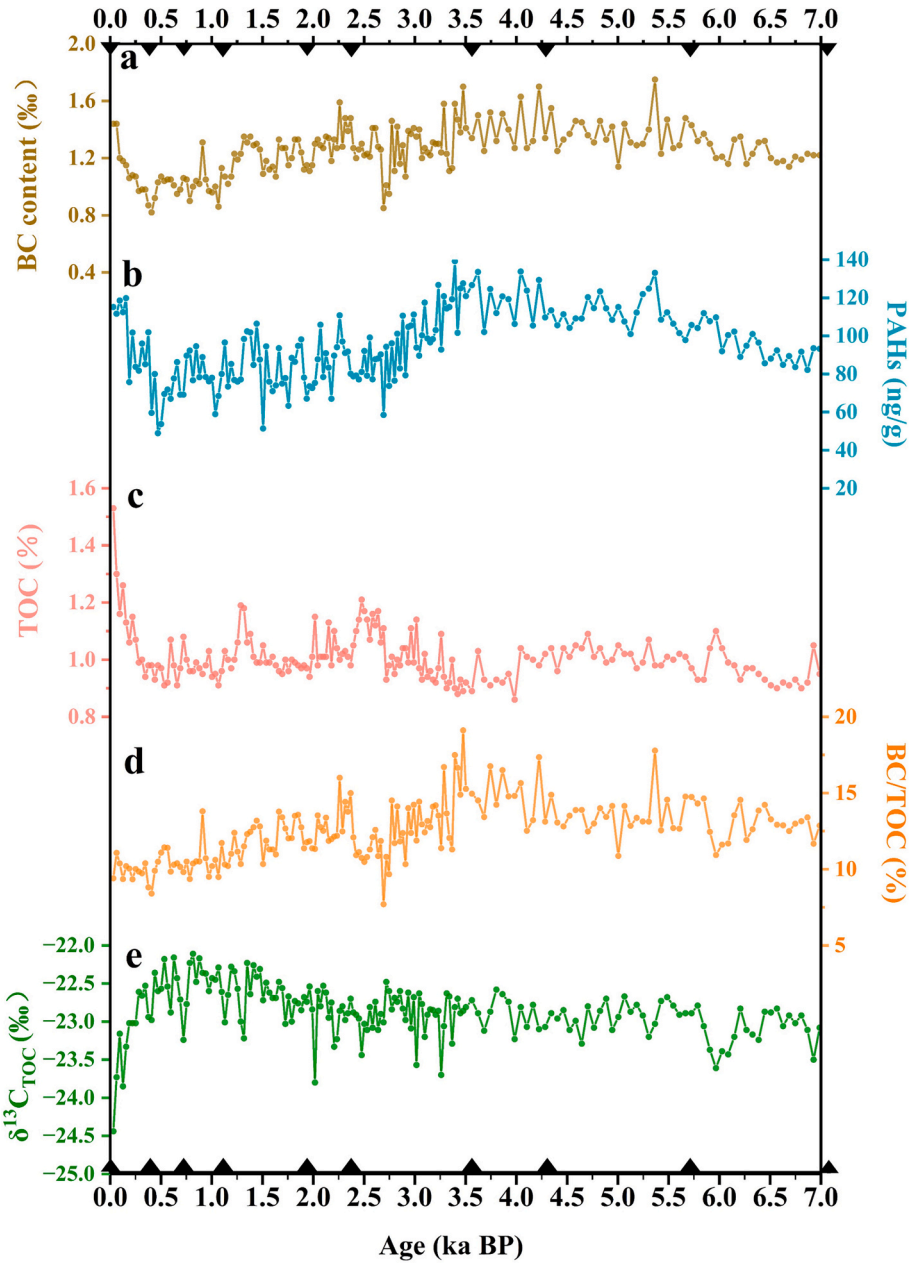

Fig. 7. Comparison of the records of fire activity with carbon sequestration since 7.0 ka BP. (a) BC content (‰) of core YS-A; (b) PAHs content (ng/g) of core YS-A; (c) TOC content (%) of core YS-A; (d) BC/TOC ratio (%) of core YS-A; (e) $\delta^{13}C_{TOC}$ (‰) of core YS-A. The black triangles are age control points.

reveals that fire activity gradually increased during 7.0–4.0 ka BP, reaching its peak around 4.0–3.5 ka BP, and subsequently weakened during 3.5–0.5 ka BP, finally showed a rapid increasing trend since 0.5 ka BP. Our findings suggest that climate change has been the dominant factor influencing fire history in the Yellow River Basin since 7.0 ka BP. Specifically, drier climate promoted fire activity before 4.0 ka BP, but suppressed fire activity after 4.0 ka BP. We speculate that the response of fire to climatic conditions may depend heavily on whether vegetation cover limits fire occurrence at this time. Furthermore, human activities have also played a role in reducing vegetation cover through deforestation and restrained fire activity since the Late Holocene on a millennium scale. However, a significant increase in human activity could promote more biomass burning during specific periods over short terms. Large-scale population migrations from the Yellow River Basin led to a decrease in fire activity during 1.9–1.8, 1.6–1.4, and 1.1–0.9 ka BP. Since 0.5 ka BP, a significant increase in wheat planting may generate more fire from C3 biomass. In particular, coal burning has increased high-temperature combustion since 0.5 ka BP. Moreover, our study

found that fire activity affected carbon sequestration in marine sediments, including increased burial of refractory carbon and the proportion of terrestrial organic matter.

CRediT authorship contribution statement

Chuchu Zhang: Writing – original draft, Methodology, Investigation, Formal analysis, Data curation, Conceptualization. **Yifei Qiu:** Visualization, Validation, Software, Formal analysis, Data curation. **Chenglong Wang:** Writing – review & editing, Resources, Project administration, Methodology. **Qinya Fan:** Software, Methodology. **Ziyue Feng:** Software, Methodology. **Xinqing Zou:** Writing – review & editing, Resources, Funding acquisition.

Declaration of competing interest

This manuscript has not been published or presented elsewhere in part or in entirety and is not under consideration by another journal. We have read and understood your journal's policies, and we believe that neither the manuscript nor the study violates any of these. There are no conflicts of interest to declare.

Data availability

Data will be made available on request.

Acknowledgement

The study was supported by the Natural Resources Science and Technology Project of Jiangsu Province (Grant No. JSZRKJ202423), the Natural Science Foundation of China (Grant Nos. 42106056), and the Fundamental Research Funds for the Central Universities (Grant Nos. 0209-14370410, 0209–14380134).

Appendix A. Supplementary data

Supplementary data to this article can be found online at https://doi.org/10.1016/j.palaeo.2024.112626.

References

Ai, L., Han, Z., Wu, X., Liu, S., Bi, N., Saito, Y., Shi, X., Wang, H., 2022. How did the climate and human activities modulate the sedimentary evolution of the Central Yellow Sea Mud, China. J. Asian Earth Sci. 235, 105299.
Alexander, C.R., Demaster, D.J., Nittrouer, C.A., 1991. Sediment accumulation in a modern epicontinental-shelf setting: the Yellow Sea. Mar. Geol. 98 (1), 51–72.
Argiriadis, E., Battistel, D., McWethy, D.B., Vecchiato, M., Kirchgeorg, T., Kehrwald, N. M., Whitlock, C., Wilmshurst, J.M., Barbante, C., 2018. Lake sediment fecal and biomass burning biomarkers provide direct evidence for prehistoric human-lit fires in New Zealand. Sci. Rep. 8.
Bird, M.I., Grocke, D.R., 1997. Determination of the abundance and carbon isotope composition of elemental carbon in sediments. Geochim. Cosmochim. Acta 61, 3413–3423.
Blaauw, M., Christen, J.A., 2011. Flexible paleoclimate age-depth models using an autoregressive gamma process. Bayesian Anal. 6.
Bond, G., Kromer, B., Beer, J., Muscheler, R., Evans, M.N., Showers, W., Hoffmann, S., LottiBond, R., Hajdas, I., Bonani, G., 2001. Persistent solar influence on North Atlantic climate during the Holocene. Science 294, 2130–2136.
Bond-Lamberty, B., Peckham, S.D., Ahl, D.E., Gower, S.T., 2007. Fire as the dominant driver of Central Canadian boreal forest carbon balance. Nature 450, 89–92.
Bowman, D.M.J.S., Balch, J.K., Artaxo, P., Bond, W.J., Carlson, J.M., Cochrane, M.A., D'Antonio, C.M., DeFries, R.S., Doyle, J.C., Harrison, S.P., Johnston, F.H., Keeley, J. E., Krawchuk, M.A., Kull, C.A., Marston, J.B., Moritz, M.A., Prentice, I.C., Roos, C.I., Scott, A.C., Swetnam, T.W., van der Werf, G.R., Pyne, S.J., 2009. Fire in the earth system. Science, 324, 481–484.
Bowman, D.M.J.S., Williamson, G.J., Abatzoglou, J.T., Kolden, C.A., Cochrane, M.A., Smith, A.M.S., 2017. Human exposure and sensitivity to globally extreme wildfire events. Nat. Ecol. Evol. 1.
Burns, W.A., Mankiewicz, P.J., Bence, A.E., Page, D.S., Parker, K.R., 1997. A principal-component and least-squares method for allocating polycyclic aromatic hydrocarbons in sediment to multiple sources. Environ. Toxicol. Chem. 16, 1119–1131.
Chen, F., Xu, Q., Chen, J., Birks, H.J.B., Liu, J., Zhang, S., 2015. East Asian summer monsoon precipitation variability since the last deglaciation. Sci. Rep. 5 (1).
Chen, Z., Wan, S., Zhang, J., Huang, J., Liu, S., Li, A., 2021. Evolution of C3/C4 vegetation in eastern China since the late Pliocene: evidence from black carbon record in the South Yellow Sea. Quat. Sci. 41, 948–964.
Chen, Z., Wan, S., Zhang, J., Zhao, D., Huang, J., Pei, W., Li, M., Shi, X., Li, A., 2022. Human impact overwhelms long-term climatic control on c4 vegetation in the yellow river basin after 3 ka BP. Geosyst. Geoenviron. 1 (2).
Cheng, F., 2010. The Study on Agricultural Development of Livelihood of Shandong Province. Nankai University, China, Tianjin.
Daniau, A.L., Harrison, S.P., Bartlein, P.J., 2010. Fire regimes during the last Glacial. Quat. Sci. Rev. 29, 2918–2930.
Daniau, A., Sánchez Goñi, M.F., Martinez, P., Urrego, D.H., Bout-Roumazeilles, V., Desprat, S., Marlon, J.R., 2013. Orbital-scale climate forcing of grassland burning in southern Africa. Proc. Natl. Acad. Sci. 110, 5069–5073.
Finsinger, W., Fevre, J., Orban, I., Pal, I., Vincze, I., Hubay, K., Birks, H.H., Braun, M., Toth, M., Magyari, E.K., 2016. Holocene fire-regime changes near the treeline in the Retezat Mts. (Southern Carpathians, Romania). Quat. Int. 94–105.
Garcés-Pastor, S., Coissac, E., Lavergne, S., et al., 2022. High resolution ancient sedimentary DNA shows that alpine plant diversity is associated with human land use and climate change. Nat. Commun. 13.
Hamer, U., Marschner, B., Brodowski, S., Amelung, W., 2004. Interactive priming of black carbon and glucose mineralisation. Org. Geochem. 35, 823–830.
Hammes, K., Schmidt, M.W.I., Smernik, R.J., Currie, L.A., Ball, W.P., et al., 2007. Comparison of quantification methods to measure fire-derived (black/elemental) carbon in soils and sediments using reference materials from soil, water, sediment and the atmosphere. Glob. Biogeochem. Cycles 21, GB3016.
Han, Y.M., Marlon, J.R., Cao, J.J., Jin, Z.D., An, Z.S., 2012. Holocene linkages between char, soot, biomass burning and climate from Lake Daihai, China. Glob. Biogeochem. Cycles 26.
Hao, W., Ward, D., Olbu, G., Baker, S., 1996. Emissions of CO2, CO, and hydrocarbons from fires in diverse African savanna ecosystems. J. Geophys. Res. Atmos. 1996 (101), 23577–23584.
Heymann, J., Reuter, M., Buchwitz, M., Schneising, O., Bovensmann, H., Burrows, J.P., Massart, S., Kaiser, J.W., Crisp, D., 2017. CO_2 emission of Indonesian fires in 2015 estimated from satellite-derived atmospheric CO_2 concentrations. Geophys. Res. Lett. 44, 1537–1544.
Hou, G.L., Fang, X.Q., 2012. Characteristics analysis and synthetical reconstruction of regional temperature series of the Holocene in China. J. Palaeogeogr. 14, 243–252.
Huang, C.C., Pang, J.L., Chen, S., Su, H., Han, J., Cao, Y., et al., 2006. Charcoal records of fire history in the Holocene loess-soil sequences over the southern Loess Plateau of China. Palaeogeogr. Palaeoclimatol. Palaeoecol. 239 (1–2), 28–44.
Huang, C.C., Pang, J.L., Su, H.X., Li, S.L., Ge, B.W., 2009. Holocene environmental change inferred from the loess-palaeosol sequences adjacent to the floodplain of the Yellow River, China. Quat. Sci. Rev. 28, 2633–2646.
Huang, Z., Ma, C., Chyi, S.J., Tang, L., Zhao, L., 2020. Paleofire, Vegetation, and climate Reconstructions of the Middle to late Holocene from Lacustrine Sediments of the Toushe Basin, Taiwan. Geophys. Res. Lett. 47.
Huang, X., Ding, K., Liu, J., Wang, Z., Tang, R., Xue, L., Wang, H., Zhang, Q., Tan, Z., Fu, C., Davis, S.J., Andreae, M.O., Ding, A., 2023. Smoke-weather interaction affects extreme wildfires in diverse coastal regions. Science 379, 457–461.
Keeley, J.E., Bond, W.J., Bradstock, R.A., Pausas, J.G., Rundel, P.W., 2011. Fire in Mediterranean Ecosystems: Ecology, Evolution and Management. Cambridge University Press, Cambridge.
Krawchuk, M.A., Moritz, M.A., Parisien, M., Van Dorn, J., Hayhoe, K., 2009. Global Pyrogeography: the current and Future distribution of Wildfire. PLoS ONE 4, 1–12.
Lelieveld, J., Evans, J.S., Fnais, M., Giannadaki, D., Pozzer, A., 2015. The contribution of outdoor air pollution sources to premature mortality on a global scale. Nature 525, 367–371.
Liu, J.P., Milliman, J.D., Gao, S., Cheng, P., 2004. Holocene development of the Yellow River's subaqueous delta, North Yellow Sea. Mar. Geol. 209, 45–67.
Liu, J., Saito, Y., Kong, X., Wang, H., Wen, C., Yang, Z., Nakashima, R., 2010. Delta development and channel incision during marine isotope stages 3 and 2 in the western South Yellow Sea. Mar. Geol. 278, 54–76.
Liu, L., Zhou, X., Yu, Y.Y., Guo, Z.T., 2011. The natural vegetation on the Loess Plateau: the evidence of soil organic carbon isotope. Quat. Sci. 31, 506–513.
Liu, L., Song, Y., Cui, L., Hao, Z., 2013. Stable carbon isotopic composition of black carbon in surface soil as a proxy for reconstructing vegetation on the Chinese Loess Plateau. Palaeogeogr. Palaeoclimatol. Palaeoecol. 388, 109–114.
Liu, X., Tang, D., Ge, C., 2020. Distribution and sources of organic carbon, nitrogen and their isotopic composition in surface sediments from the southern Yellow Sea, China. Mar. Pollut. Bull. 150, 110716.
Liu, D., Zhou, C., Keesing, J.K., Serrano, O., Werner, A., Fang, Y., Chen, Y., Masque, P., Kinloch, J., Sadekov, A., Du, Y., 2022. Wildfires enhance phytoplankton production in tropical oceans. Nat. Commun. 13.
Marlon, J.R., Bartlein, P.J., Carcaillet, C., Gavin, D.G., Harrison, S.P., Higuera, P.E., Joos, F., Power, M.J., Prentice, I.C., 2008. Climate and human influences on global biomass burning over the past two millennia. Nat. Geosci. 1, 697–702.
Menzie, C.A., Potocki, B.B., Santodonato, J., 1992. Exposure to carcino-genic PAH in the environment. Environ. Sci. Technol. 1 (7), 278–1284.
Milliman, J.D., Farnsworth, K.L., 2011. River Discharge to the Coastal Ocean: A Global Synthesis. Cambridge University Press, Cambridge.
Mitra, S., Zimmerman, A.R., Hunsinger, G.B., Willard, D., Dunn, J.C., 2009. A Holocene record of climate-driven shifts in coastal carbon sequestration. Geophys. Res. Lett. 36.

Mu, Y., Qin, X., Zhang, L., Xu, B., 2017. Link between black carbon, fires, climate change, and human activity during the Holocene period shown in the loess-paleosol sequence from Henan, China. Quat. Res. 87 (2), 288–297.
Ning, D., Jiang, Q., Ji, M., Zheng, J., Kuai, X., Ge, Y., et al., 2022. Sedimentary Black Carbon isotope record of Holocene climate changes on the northeastern Tibetan Plateau. Paleoceanogr. Paleoclimatol. 37, e2022PA004487.
Pang, Y., Zhou, B., Zhou, X., Xu, X., Liu, X., Zhan, T., Lu, Y., 2021. Abundance and $\delta^{13}C$ of sedimentary black carbon indicate rising wildfire and C4 plants in Northeast China during the early Holocene. Palaeogeogr. Palaeoclimatol. Palaeoecol. 562, 110075.
Pei, Q., Zhang, D.D., Lee, H.F., 2016. Contextualizing human migration in different agro-ecological zones in ancient China. Quat. Int. 426, 65–74.
Pei, W., Wan, S., Clift, P.D., Dong, J., Liu, X., Lu, J., Tan, Y., Shi, X., Li, A., 2020. Human impact overwhelms long-term climate control of fire in the Yangtze River Basin since 3.0 ka BP. Quat. Sci. Rev. 230, 106165.
Price, C., 2009. Will a drier climate result in more lightning? Atmos. Res. 91, 479–484.
Ren, P., Liu, Y., Shi, X., Sun, S., Fan, D., Wang, X., 2019. Sources and sink of black carbon in Arctic Ocean sediments. Sci. Total Environ. 689, 912–920.
Saito, Y., Yang, Z.S., Hori, K., 2001. The Huanghe (Yellow River) and Changjiang (Yangtze River) deltas: a review on their characteristics, evolution and sediment discharge during the Holocene. Geomorphology 41, 219–231.
Sankey, J.B., Germino, M.J., Glenn, N.F., 2009. Aeolian sediment transport following wildfire in sagebrush steppe. J. Arid Environ. 73, 912–919.
Scholze, M., Knorr, W., Arnell, N.W., Prentice, I.C., 2006. A climate-change risk analysis for world ecosystems. Proc. Natl. Acad. Sci. 103, 13116–13120.
Scott, A.C., 2000. The Pre-Quaternary history of fire. Palaeogeogr. Palaeoclimatol. Palaeoecol. 164, 281–329.
Scott, A.C., Glasspool, I.J., 2006. The diversification of Paleozoic fire systems and fluctuations in atmospheric oxygen concentration. Proc. Natl. Acad. Sci. 103, 10861–10865.
Shi, N.H., 1991. On the historical distributions and vicissitudes of national vegetation of China. Coll. Essays Chin. Hist. Geogr. 3, 43–74.
Sun, X., Hu, L., Hu, B., Sun, X., Wu, X., Bi, N., Lin, T., Guo, Z., Yang, Z., 2022a. Remarkable signals of the ancient Chinese civilization since the early Bronze Age in the marine environment. Sci. Total Environ. 804, 150209.
Sun, Y., Zhang, S., Xu, Q., 2022b. Pollen-based land cover changes reveal temporal and spatial differences of human activity in north-Central China during the Holocene. Catena 219, 106620.
Tan, Z., Han, Y., Cao, J., Chang Huang, C., An, Z., 2015. Holocene wildfire history and human activity from high-resolution charcoal and elemental black carbon records in the Guanzhong Basin of the Loess Plateau, China. Quat. Sci. Rev. 109, 76–87.
Tan, Z., Wu, C., Han, Y., Zhang, Y., Mao, L., Li, D., Liu, L., Su, G., Yan, T., 2020. Fire history and human activity revealed through poly cyclic aromatic hydrocarbon (PAH) records at archaeological sites in the middle reaches of the Yellow River drainage basin, China. Palaeogeogr. Palaeoclimatol. Palaeoecol. 560, 110015.
Tan, Z., Gu, M., Han, Y., Mao, L., Zhou, L., Liu, L., Li, S., Qin, H., Tan, T., 2022. Records of fire and its controls on coastal plain of Laizhou Bay, China since 5000 years. Palaeogeogr. Palaeoclimatol. Palaeoecol. 585, 110702.
Tang, W., Llort, J., Weis, J., Perron, M.M.G., Basart, S., Li, Z., Sathyendranath, S., Jackson, T., Sanz Rodriguez, E., Proemse, B.C., Bowie, A.R., Schallenberg, C., Strutton, P.G., Matear, R., Cassar, N., 2021. Widespread phytoplankton blooms triggered by 2019-2020 Australian wildfires. Nature 597, 370–375.
Thevenon, F., Williamson, D., Bard, E., Anselmetti, F.S., Beaufort, L., Cachier, H., 2010. Combining charcoal and elemental black carbon analysis in sedimentary archives: Implications for past fire regimes, the pyrogenic carbon cycle, and the human-climate interactions. Glob. Planet. Chang. 72, 381–389.
Tian, H., 2018. Study on Wheat Production and Influence in the Middle and Lower Reaches of the Yellow River during the Ming and Qing Dynasty. Nanjing Agricultural University.
Wang, X.C., Li, A.C., 2007. Preservation of black carbon in the shelf sediments of the East China Sea. Chin. Sci. Bull. 52, 3155–3161.
Wang, L., Shao, M.A., Wang, Q., Gale, W.J., 2006. Historical changes in the environment of the Chinese Loess Plateau. Environ. Sci. Pol. 9, 675–684.
Wang, Y., Cheng, H., Edwards, R.L., Kong, X., Shao, X., Chen, S., Wu, J., Jiang, X., Wang, X., An, Z., 2008. Millennial- and orbital-scale changes in the East Asian monsoon over the past 224,000 years. Nature 451, 1090–1093.
Wang, X., Ding, Z., Peng, P., 2012. Changes in fire regimes on the Chinese Loess Plateau since the last glacial maximum and implications for linkages to paleoclimate and past human activity. Palaeogeogr. Palaeoclimatol. Palaeoecol. 315-316, 61–74.
Wang, X., Cui, L., Xiao, J., Ding, Z., 2013. Stable carbon isotope of black carbon in Lake sediments as an indicator of terrestrial environmental changes: an evaluation on paleorecord from Daihai Lake, Inner Mongolia, China. Chem. Geol. 347, 123–134.
Wang, Y., Shen, C., Shen, Z., Zhang, D., Crittenden, J.C., 2015. Spatial variation and sources of polycyclic aromatic hydrocarbons (PAHs) in surface sediments from the Yangtze Estuary, China. Environ Sci Process Impacts 17 (7), 1340–1347.
Wang, X., Cui, L., Yang, S., Zhai, J., Ding, Z., 2018. Stable carbon isotope records of black carbon on Chinese Loess Plateau since last glacial maximum: An evaluation on their usefulness for paleorainfall and paleovegetation reconstruction. Palaeogeogr. Palaeoclimatol. Palaeoecol. 509, 98–104.
Whitlock, C., Dellasala, D.A., Wolf, S., Hanson, C.T., 2015. Climate Change: Uncertainties, Shifting Baselines, and Fire Management.
Williams, E., Rosenfeld, D., Madden, N., Gerlach, J., Gears, N., Atkinson, L., Dunnemann, N., et al., 2002. Contrasting convective regimes over the Amazon: implications for cloud electrification. J. Geophys. Res. Atmos. 107. LBA50-51-LBA 50-19.
Wu, X., 2010. Basic historical context of coal mines in ancient China and main features of coal development and utilization. J. China Univ. Min. Technol. 12 (03), 91–98.
Xiao, J., Xu, Q., Nakamura, T., Yang, X., Liang, W., Inouchi, Y., 2004. Holocene vegetation variation in the Daihai Lake region of north-Central China: a direct indication of the Asian monsoon climatic history. Quat. Sci. Rev. 23 (14–15), 1669–1679.
Yang, Z.S., Liu, J.P., 2007. A unique Yellow River-derived distal subaqueous delta in the Yellow Sea. Mar. Geol. 240 (1–4), 169–176.
Yang, S.Y., Jung, H.S., Lim, D.I., Li, C.X., 2003. A review on the provenance discrimination of sediments in the Yellow Sea. Earth Sci. Rev. 63, 93–120.
Yuan, D., Zhu, J., Li, C., Hu, D., 2008. Cross-shelf circulation in the Yellow and East China Seas indicated by MODIS satellite observations. J. Mar. Syst. 70, 134–149.
Yunker, M.B., Macdonald, R.W., Vingarzan, R., Mitchell, R.H., Goyette, D., Sylvestre, S., 2002. PAHs in the Fraser River basin: a critical appraisal of PAH ratios as indicators of PAH source and composition. Org. Geochem. 33, 489–515.
Zhang, P., Cheng, H., Edwards, R.L., Chen, F., Wang, Y., Yang, X., Liu, J., Tan, M., Wang, X., Liu, J., 2008. A test of climate, sun, and culture relationships from an1810-year Chinese cave record. Science 322, 940–942.
Zhang, J., Liu, J., Wang, H., Xu, G., Qiu, J., Yue, B., Zhao, G., 2013. Characteristics and provenance implication of detrital minerals since marine isotope stage 3 in core SYS-0701 in the western South Huanghai Sea. Acta Oceanol. Sin. 32, 49–58.
Zhang, Z., Zhong, J., Lv, X., Tong, S., Wang, G., 2015. Climate, vegetation, and human influences on late-Holocene fire regimes in the Sanjiang plain, northeastern China. Palaeogeogr. Palaeoclimatol. Palaeoecol. 438, 1–8.
Zhang, C., Qiu, Y., Dong, Z., Wang, C., Wang, Y., Liao, Q., Zou, X., 2024. Natural and anthropogenic forcing on the fate of sedimentary organic matter in the South Yellow Sea during the Holocene. Palaeogeogr. Palaeoclimatol. Palaeoecol. 634, 111958.
Zhao, Y., Yu, Z., Chen, F., Zhang, J., Yang, B., 2009. Vegetation response to Holocene climate change in monsoon-influenced region of China. Earth Sci. Rev. 97 (1–4), 242–256.
Zhao, G., Mu, X., Wen, Z., Wang, F., Gao, P., 2013. Soil erosion, conservation, and eco-environmental changes in the Loess Plateau of China. Land Degrad. Dev. 24, 499–510.
Zheng, B., Ciais, P., Chevallier, F., Yang, H., Canadell, J.G., Chen, Y., van der Velde, I.R., Aben, I., Chuvieco, E., Davis, S.J., Deeter, M., Hong, C., Kong, Y., Li, H., Li, H., Lin, X., He, K., Zhang, Q., 2023. Record-high CO_2 emissions from boreal fires in 2021. Science 379, 912–917.
Zheng, X., Sun, N., Luo, F., 2024. Spatio-temporal feature of active fire occurrence on the Loess Plateau from 2001 to 2020 based on Modis. Quat. Sci. 44 (1), 191–200.
Zhou, B., Shen, C., Sun, W., Zheng, H., Yang, Y., Sun, Y., An, Z., 2007. Elemental carbon record of paleofire history on the Chinese Loess Plateau during the last 420 ka and its response to environmental and climate changes. Palaeogeogr. Palaeoclimatol. Palaeoecol. 252, 617–625.
Zong, Y., Chen, Z., Innes, J.B., Chen, C., Wang, Z., Wang, H., 2007. Fire and flood management of coastal swamp enabled first rice paddy cultivation in East China. Nature 449, 459–462.